Non-competitive resource exploitation within-mosquito shapes evolution of malaria virulence

G. Costa[1], M. Gildenhard[1#], M. Eldering[1,2#], R.L. Lindquist[3], A.E. Hauser[3,4], R. Sauerwein[2], C. Goosmann[1], V. Brinkmann[1] and E.A. Levashina[1*]

Affiliations:

[1] Max Planck Institute for Infection Biology, Berlin, Germany

[2] Radboud University Medical Center, Nijmegen, The Netherlands

[3] German Rheumatism Research Centre (DRFZ), Berlin, Germany

[4] Charité-Universitätsmedizin Berlin, Germany

[#] These authors contributed equally to this work

* Corresponding author: levashina@mpiib-berlin.mpg.de

Abstract

Malaria is a fatal human parasitic disease transmitted by a mosquito vector. The evolution of within-host malaria virulence has been the focus of many empirical and theoretical studies. However, the vector's contribution to virulence evolution is not well understood. Here we explored how within-vector resource exploitation impacts evolutionary trajectories of within-host *Plasmodium* virulence. We developed a nested model of within-vector dynamics and malaria epidemiology, which predicted that non-competitive resource exploitation within-vector restricts within-host parasite virulence. To validate our model, we experimentally manipulated mosquito lipid trafficking and gauged within-vector parasite development, within-host infectivity and virulence. We found that mosquito-derived lipids determine within-host parasite virulence by shaping development and metabolic activity of transmissible sporozoites. Our findings uncover the role of within-vector environment in regulating within-host *Plasmodium* virulence and identify *Plasmodium* metabolic traits that may contribute to the evolution of malaria virulence.

INTRODUCTION

Malaria is caused by the vector-borne protozoan parasite *Plasmodium falciparum* and kills 429,000 people annually, predominantly in sub-Saharan Africa[1]. The unacceptably high malaria mortality is tightly linked to within-host parasite virulence (here defined as capacity to cause harm to the human host). Therefore, predicting the evolution of *Plasmodium* virulence has important epidemiological, socio-medical and evolutionary implications for designing malaria control strategies. The life cycle of malaria parasites is split between the host and the mosquito vector. Theoretical and empirical studies focused on regulation of within-host malaria virulence, including contributions of parasite genetic factors and host immune responses, and on the link between virulence and host-to-vector transmission[2-4]. The latter reports showed that genetically-encoded within-host parasite virulence increases the production of infective to vector forms and, thereby, parasite transmission to the vector[5]. Females of anopheline mosquitoes feed on blood to initiate ovary development. Therefore, only females ingest *Plasmodium* and contribute to malaria transmission. During a blood meal, blood-borne sexual forms of parasites fuse to form motile zygotes that within two days after infection traverse the midgut epithelium, reach the basal side of the midgut to round-up into oocysts. In the next 10-15 days, each oocyst undergoes sporogony, a process that generates thousands sporozoites, the parasite stage infective to humans. Sporozoites egress from the oocysts and migrate to the mosquito salivary glands to reach full maturity and infectivity[6]. Nutrients taken up by female mosquitoes during a blood meal are essential for vector reproduction and for massive *Plasmodium* proliferation at the oocyst stage[7,8]. Although many studies examined associations between *Plasmodium* virulence and vector fitness, only a few reported significant changes in longevity and fecundity of *Plasmodium*-infected mosquitoes, thus precluding generalized conclusions[9-13]. Whether within-vector resource exploitation by parasites modulates within-host malaria virulence has never been explored.

Here we applied theoretical and experimental approaches to examine the link between parasite within-vector resource exploitation and virulence towards the mammalian host. We modeled alternative scenarios of vector-parasite symbiosis and investigated their consequences for parasite transmission dynamics. Our modeling results predicted that vector-parasite relationship of resource acquisition shapes the evolution of within-host virulence. A parasitic relationship, where the parasite exploited vector mechanisms to

scavenge resources, restricted parasite virulence, whereas virulence runaway was observed in a competitive relationship. To test these predictions, we experimentally manipulated lipid trafficking in genetically identical mosquitoes and exploited a rodent malaria model to gauge the impact of these manipulations on within-host virulence of genetically identical parasites. We found that mosquito-derived lipids determine within-host *Plasmodium* virulence by shaping sporogony and metabolic activity of sporozoites. By showing that evolution of malaria virulence is metabolically regulated by the within-vector nutritional environment, our findings have important implications for vector control strategies based on biological competitors or on manipulation of mosquito reproduction.

RESULTS

Within-vector environment shapes evolution of within-host malaria virulence

To test for the evolutionary consequences of a trade-off between mosquito reproduction, parasite reproduction and virulence, we used a modeling approach by considering a within-vector dynamics model in an epidemiological framework (Materials and Methods). We modeled within-vector resource competition between mosquito reproduction (egg production) and parasite reproduction (sporozoite load) as a competitive Lotka-Volterra equation[14,15]. This model describes egg production, parasite production and the competition strength between vector and parasite α_{EP} and α_{PE} (their ability to inhibit each other's growth). Mechanistically, the parasite's competition coefficient represents its within-vector resource scavenging and, thereby, its harm towards vector reproduction.

We next combined this within-vector model with an epidemiological model for vector-borne disease, which describes human-to-vector and vector-to-human parasite transmission. Pathogen evolution can be investigated with epidemiological models, assuming that selection maximizes the parasite's ability to spread from one host to the next expressed as the basic reproductive ratio R_0. For vector-borne diseases, R_0 is the product of the vector-to-host and host-to-vector transmission potentials[16]. In line with previous reports[17-19], we postulate that virulence towards the host is influenced by within-vector resource acquisition. We specifically hypothesize that within-vector resource exploitation influences virulence by impacting parasite load and infectivity to the host (Figure 1A).

Combining within-host Lotka-Volterra dynamics with epidemiological dynamics allows us to investigate evolution of R_0 under varying parasite and vector competition coefficients. When vector and parasite use independent mechanisms to scavenge resources (competitive relationship), both competition coefficients have a positive sign ($\alpha_{EP} > 0; \alpha_{PE} > 0$), reflecting a reciprocally inhibitory competitive relationship (Figure 1B). We found that competitive environment selects for higher parasite's competition coefficient (Figure 1C), eventually leading to vector sterilization and to high levels of within-host virulence (Figure 1D). This can be explained by the fact that both vector-to-human and human-to-vector transmission rates benefit from increasing the parasite's competitiveness. When parasites mechanistically depend on the vector's investment in reproduction (parasitic relationship), the vector's competition coefficient turns negative ($\alpha_{EP} > 0; \alpha_{PE} < 0$) (Figure 1C). We found that in contrast to the competitive scenario, the parasitic relationship leads to opposing evolutionary trajectories between the two transmission events. Indeed, higher α_{EP} decreases parasite's density and vector-to-human transmission but increases human-to-vector transmission (Figure 1E). Such a trade-off between transmission events would lead to the emergence of an evolutionarily stable malaria virulence (Figure 1C and D).

Taken together, our theoretical analyses predicted that the shape of vector-parasite relationship defines the evolutionary trajectories of within-host virulence.

Mosquito lipid environment regulates *Plasmodium* virulence in the next mammalian host

To formalize our theoretical assumption that within-host virulence is defined by within-vector resource acquisition, we examined changes in *Plasmodium* virulence after restricting within-vector lipid resources. In these experiments, we used RNAi in adult females to deplete the major mosquito lipid transporter lipophorin (Lp) without affecting mosquito diet or development[20-22]. As expected, Lp depletion prevented lipid transport between mosquito tissues, inhibited ovary and parasite development (Figure S1). We next exposed naïve mice to the bites of *P. berghei*-infected control or Lp-depleted mosquitoes. We found that Lp depletion drastically attenuated parasite infectivity and virulence. Indeed, only 20% of mice bitten by Lp-depleted mosquitoes became infected

112 and only 10% developed severe neurological symptoms of experimental cerebral
113 malaria (ECM) compared to 90% in controls (Figure 2A-C). As the observed phenotypes
114 could result from the differences in numbers of inoculated parasites, we subcutaneously
115 injected naïve mice with equal quantities of sporozoites isolated from control and Lp-
116 depleted mosquitoes. Again, fewer than 40% of mice injected with lipid-deprived
117 sporozoites became infected and only 20% of mice developed ECM, as compared to
118 100% in controls (Figure 2D-F). These results confirm the major assumption of our
119 model and show that the within-vector lipid environment impacts within-host parasite
120 virulence.

121

122 ***Plasmodium* parasitizes mosquito lipids for productive sporogony and formation**
123 **of infective sporozoites**

124 Our theoretical study predicted that the type of symbiotic relationship (competitive or
125 parasitic) defines the evolutionary trajectory of parasite virulence. As restricting
126 trafficking of lipid resources impacted virulence, we examined the parasitic scenario,
127 where *Plasmodium* exploits mosquito Lp for lipid delivery. We microscopically gauged
128 lipid accumulation and parasite growth using Nile Red lipid staining, and observed
129 accumulation of neutral lipids in the peripheral cytoplasm and vesicles of mature oocysts
130 in control mosquitoes. In contrast, levels of Nile Red staining were significantly lower in
131 the oocysts of Lp-depleted females (Figure 3A and B). Moreover, the
132 immunofluorescence analysis with anti-Lp antibodies in controls showed an increase in
133 the rate of Lp-positive oocysts from 25% to 72% at 7 and 13 days post infection (dpi),
134 respectively (Figure S2). These results support the parasitic scenario, in which
135 *Plasmodium* exploits Lp for lipid delivery to its proliferating stages. Depletion of Lp
136 inhibited oocyst sporulation, caused abnormal cytoplasmic vacuolizations (Figure 3C
137 and Figure S3), and significantly reduced the size of mature oocysts (Figure 3D). In line
138 with these results, perturbation of lipid trafficking decreased the density of transmissible
139 sporozoites (Figure 3E). Similar results were obtained with the human malaria parasite
140 *P. falciparum* (Figure 3D and E), suggesting that within-vector parasitic relationships are
141 conserved between human and rodent *Plasmodium* species.

142 As lipid restriction attenuated within-host virulence, we set out to identify *Plasmodium*
143 traits affected by Lp depletion. In these experiments, we compared morphology, vitality

144 and gene expression of the sporozoites produced by control and Lp-depleted
145 mosquitoes. We found that lipid-deprived sporozoites were alive and properly expressed
146 major maturation markers (Figure 3F and Figure S4). As lipids are crucial for metabolic
147 activity, we measured mitochondrial membrane potential using TMRE dye, which
148 accumulates in the membrane matrix of active mitochondria[23]. Lipid-deprived
149 sporozoites showed a significant decrease in mitochondrial membrane potential
150 compared to controls (Figure 3G and Figure S4), suggesting that mosquito lipids shape
151 metabolic activity of *Plasmodium* transmissible forms. Moreover, TMRE intensities in
152 control sporozoites were broadly distributed over a range of 2.5 logs, as opposed to a
153 sharp peak of the cytoplasmic GFP signal (Figure 3F and G). These results suggest that
154 genetically identical sporozoites display high variability in mitochondrial activity, which
155 may contribute to the plasticity of within-host virulence. Taken together, our data provide
156 experimental evidence that *Plasmodium* exploits Lp to scavenge mosquito lipid
157 resources for its within-vector proliferation in a non-competitive parasitic manner, and
158 identify mitochondrial membrane potential as a virulence-associated trait.

159

160 **Time-shift in *Plasmodium* sporulation circumvents competition for mosquito**
161 **resources**

162 What mechanism allows the parasites to avoid competition for the vector's resource
163 investment in reproduction? To answer this question, we gauged the timing of lipid
164 consumption by the mosquito ovaries and of parasite proliferation. We observed a clear
165 temporal shift between these two processes. While mosquito ovaries accumulated lipids
166 within the first two days after feeding, *Plasmodium* proliferation began one week post-
167 infection (Figure 4A). We hypothesized that in order to avoid a direct competition for
168 nutrients, *Plasmodium* could have evolved to delay its replication until after completion of
169 vector's oogenesis. This time-shift hypothesis is compatible with the non-competitive
170 parasitic scenario where parasites benefit from lipid delivery after completion of
171 oogenesis, as long as sufficient resources are left for parasite development. Therefore, if
172 lipid restriction affected only replicating oocysts, providing lipids at the initiation of oocyst
173 sporogony should bypass one week of lipid starvation and rescue parasite development
174 and virulence. We tested this hypothesis by directly gauging sporozoite infectivity and
175 development into extra-erythrocytic forms (EEFs) in the hepatoma HepG2 cells *in vitro*.

176 Cells were exposed to equal numbers of sporozoites isolated from control and Lp-
177 depleted mosquitoes that received (Figure 4Bv-viii) or not (Figure 4Bi-iv) a supplemental
178 blood feeding seven days post infection, at the time when the first effects of lipid
179 starvation on the oocyst's size were observed (Figure 3C and Figure S3). EEF
180 development was examined by fluorescence microscopy. As expected for a single blood
181 feeding, lipid restriction attenuated sporozoite numbers, infectivity and development *in*
182 *vitro*, as significantly smaller EEFs were produced by lipid-deprived sporozoites
183 compared to controls (Figure 4Bi-iv and Figure S5). Strikingly, the supplemental feeding
184 restored sporozoite numbers in Lp-depleted mosquitoes, as well as parasite infectivity
185 and EEF development (Figure 4Bv-viii and Figure S5). Our data show that delivering
186 lipids to the oocysts after completion of vector's oogenesis rescues *Plasmodium*
187 infectivity and virulence. Taken together, these results suggest that a time-shift in
188 *Plasmodium* sporogony circumvents within-vector competition for reproductive
189 resources.

190

191 **DISCUSSION**

192 Virulence is one of the most evolutionarily relevant and complex pathogen traits.
193 Understanding virulence mechanisms provides an opportunity to predict and, potentially
194 control the pathogen burden and its evolution. Here we generated theoretical models of
195 the mosquito-parasite relationship, experimentally evaluated them, and found that
196 *Plasmodium* hijacks the main mosquito lipid transporter for lipid delivery to the actively
197 proliferating oocysts after completion of the vector reproductive cycle. Such time-shift in
198 oocyst maturation benefits the parasitic relationship by allowing a timely allocation of
199 resources needed for host reproduction and for parasite proliferation. Temporal
200 regulation plays a critical role in host-parasite interactions and in host immune
201 responses. In mosquitoes, the ookinetes at the basal side of the midgut are the major
202 target of the mosquito immune system within the first 24-48 h after blood meal, whereas
203 even the earliest oocyst stages are spared from the complement attack[24]. Interestingly,
204 sporogony is the longest replicative process in the life cycle of all *Plasmodium* species
205 (12 to 16 days depending on the species). Given the average mosquito life span of 30
206 days, it roughly corresponds to a half of mosquito life. Prolongation of the within-vector
207 sejour is risky for the parasite, which should be selected to maximize its chances to

208 infect the next host as fast as possible. Therefore, the beneficial effects of lengthy
209 sporogony must be under a strong selective pressure. We predict that shifting the timing
210 of resource allocation should have dramatic consequences for parasite development,
211 transmission and virulence.

212 Our observations suggest that limited lipid resources during sporulation induce an
213 autophagy-like cell death and select for the most competitive parasites that effectively
214 scavenge nutrients from the mosquito. Autophagy, often characterized by cytoplasmic
215 vacuolization, has been observed in a large proportion of *Plasmodium* liver stages[25], and
216 our results extend these observations to the extracellular oocysts. Nutrient restriction in
217 natural conditions could be induced by oocyst crowding[19]; however in our experiments
218 the numbers of pre-sporogonic oocysts between the experimental groups were similar[21].
219 Interestingly, prolonged periods of nutrient deprivation cause cell autophagy and induce
220 mitochondrial dysfunction in mouse embryonic fibroblasts[26]. Similarly, we found that lipid
221 restriction blunted sporozoite's mitochondrial membrane potential. Mitochondria are
222 essential for mosquito stages of the *Plasmodium* life cycle, as mutations in mitochondrial
223 genes arrest growth and sporulation of oocysts[27-30]. Moreover, inhibition of mitochondrial
224 potential by the antimalarial drug atovaquone inhibits *Plasmodium* sporogonic
225 development and reduces the number and size of developing EEFs *in vitro*[31-33]. Together
226 with these findings, our results identify mitochondria as crucial regulators of within-vector
227 *Plasmodium* proliferation, transmission and within-host virulence. Although drug
228 pressure on the mitochondria frequently selects for resistance, most of the identified
229 mutations are loss-of-function, that disrupt within-vector parasite development and
230 disable transmission[30]. Therefore, *Plasmodium* mitochondria may represent an
231 evolution-proof drug target[34], as long as no gain-of-function mutations emerge that may
232 increase mitochondrial activity and, thereby, parasite virulence.

233 At the ecological level, our data show that the plasticity of parasite virulence is
234 metabolically regulated. We found that even in normal conditions, sporozoites display
235 broad variability in their mitochondrial activity. This implies that mosquito life-history traits
236 can directly influence parasite virulence. Variable trophic environments of larval breeding
237 sites[35] and of blood meals should translate inter-individual mosquito nutritional
238 differences into variability in *Plasmodium* virulence. Indeed, multiple reports have
239 implicated larval diet and adult blood meals in determining parasite loads within a
240 mosquito[18,36-40], but this has not been linked to within-vector modulation of parasite

metabolic activity and within-host virulence. Our findings open up a new perspective on mosquito transmission capacity and on evolution of malaria virulence.

The evolutionary responses to vector control measures are often non-linear due to complexity of vector-parasite relationships. Competitive within-vector *Plasmodium* dynamics may result in a virulence runaway, leading to a competitive exclusion between vector and parasite and exacerbating within-host virulence. We show that parasitic non-competitive exploitation of vector lipid resources restricts evolution of *Plasmodium* virulence. Importantly, harm towards the vector's reproduction alone does not restrict virulence evolution[41]. The trade-off between within-vector parasite density and within-host virulence that restrains virulence at intermediate levels, emerges only when parasite resource acquisition depends on vector mechanisms. We provide empirical evidence that within-vector *Plasmodium* development relies on the major vector lipid transporter and that competition between vector and parasite is prevented by a time-shift between vector oogenesis and parasite sporogony. This beneficial developmental niche should be retained as long as nutrient supply is sufficient. In a low nutrient environment, the relationship may switch towards competition, which would rapidly invert the trajectory of virulence evolution. Further investigation of the effects of other mosquito factors on parasite resource acquisition is necessary to predict potential switches between parasitic and competitive vector-parasite relationships. Such situations could arise from targeting mosquito reproduction factors essential for parasite development by transgenic approaches[42], or from introduction of such biological competitors as *Wolbachia*[43]. All together our data highlight the links between metabolism and life-history traits of vector and parasite, that shape evolutionary trajectories of malaria virulence. Further theoretical, experimental, and field studies are needed to determine the effects of natural and artificial perturbations of vector and parasite metabolism on malaria epidemiology.

MATERIALS AND METHODS

Mathematical modeling

Within-vector dynamics

Vector and parasite compete for resources from a single blood meal (non-replenished nutrient source). To investigate how vector-parasite relationship shapes within-host virulence, we first modeled resource competition between vector reproduction and sporozoite development. For this purpose, we use a Lottka-Volterra competition model[14,15], considering inter- and intraspecific competition between mosquito eggs (*E*) and parasites (*P*):

$$\dot{E} = r_1 E \left(1 - \frac{E + \alpha_{EP} P}{K_E}\right) \quad (1)$$

$$\dot{P} = r_2 P \left(1 - \frac{P + \alpha_{PE} E}{K_P}\right), \quad (2)$$

where r_1 and r_2 represent the maximum intrinsic growth rate of eggs and parasites, respectively, and α_{EP} and α_{PE} describe their competition strength. The maximum egg and sporozoite densities are given by the carrying capacities K_E and K_P, which from this point on we assume to be 1.

The four equilibrium points are given by

$$\begin{pmatrix} E \to 0 & P \to 0 \\ E \to \frac{-1 + \alpha_{EP}}{-1 + \alpha_{EP}\alpha_{PE}} & P \to \frac{-1 + \alpha_{PE}}{-1 + \alpha_{EP}\alpha_{PE}} \\ E \to 0 & P \to 1 \\ E \to 1 & P \to 0 \end{pmatrix} \quad (3)$$

and describe three qualitatively different scenarios: extinction of both species, competitive exclusion, or co-existence. Because both eggs and parasites are found in the mosquito, we hereafter only focus on the non-trivial steady state, i.e., co-existence, which can only occur if both growth rates (r_1 and r_2) are positive and neither species outcompetes the other, i.e., if α_{EP} and α_{PE} are smaller than 1.

For all cases, where $0 < \alpha_{EP} < 1;\ and\ 0 < \alpha_{PE} < 1,$ sporozoite production $\bar{P}$ decreases with increasing values of α_{EP}, and increases with increasing values of α_{EP} for all, where

$0 < \alpha_{EP} < 1$; $0 > \alpha_{PE} < 1$ (Figure S6). Instead, vector reproduction $\bar{E}$ should decrease with increasing levels of α_{EP} independent of the sign of α_{PE} (Figure S7).

Epidemiological dynamics

Following Alizon and van Baalen[16], *Plasmodium* epidemiological reproductive ratio R_0 is a product of vector-to-host $v \rightarrow h$ and host-to-vector $h \rightarrow v$ transmission rates β, and of the availability of susceptible hosts S. These are constrained by the respective duration of infection defined by parasite induced mortality ϑ, recovery rate γ, and intrinsic host mortality μ:

$$Ro = \frac{\beta_{v\rightarrow h}}{\mu_v+\vartheta_v+\gamma_v} S_v * \frac{\beta_{h\rightarrow v}}{\mu_h+\vartheta_h+\gamma_h} S_h. \quad (4)$$

Nested model

To integrate the within-vector dynamics into an epidemiological model of malaria transmission, we first assumed that within-vector sporozoite production is at equilibrium before the time of transmission (i.e., quasi-steady state). Because vector-to-human transmission rate increases with the number of produced sporozoite[44], we next postulated that vector-to-human transmission rate is a linear function of equilibrium parasite density $\beta_{v\rightarrow h}(\tilde{P})$:

$$\beta_{v\rightarrow h}(\tilde{P}) = \theta_{\beta_{v\rightarrow h}} \frac{-1+\alpha_{PE}}{-1+\alpha_{EP}\alpha_{PE}}, \quad (5)$$

where $\theta_{\beta_{v\rightarrow h}}$ is a constant which describes the maximum transmission rate in relation to parasite density.

Host-to-vector transmission depends on the parasites asexual replication and production of sexual forms (gametocytes)[5,45]. Virulence towards the host is caused by the asexual production during the blood stages, which makes host-to-vector transmission a linear function of virulence $\beta_{h\rightarrow v}(\vartheta_h)$. We assume that the capacity to enter the asexual cycle depends on initial parasite load, which links parasite density at the time of vector to human transmission to human to vector transmission:

$$\beta_{h\rightarrow v}\left(\vartheta_h(\tilde{P})\right) = \theta_{\beta_{h\rightarrow v}}\theta_{\vartheta_h} \frac{-1+\alpha_{PE}}{-1+\alpha_{EP}\alpha_{PE}}, \quad (6)$$

320 where θ_{ϑ_h} and $\theta_{\beta_{v\to h}}$ are the rates for virulence and transmission in relation to parasite
321 loads. However, within-vector resource competition may also qualitatively affect the
322 parasite's capacity to infect the human host[17-19]. Therefore, we assumed that within-host
323 virulence increases with the efficiency of resource exploitation via the parasite's
324 competition coefficient:

325 $$\beta_{h\to v}\left(\vartheta_h\left(\alpha_{EP},\tilde{P}\right)\right) = \theta_{\beta_{h\to v}}\theta_{\vartheta_h}\,\alpha_{EP}\,\frac{-1+\alpha_{PE}}{-1+\alpha_{EP}\alpha_{PE}} \qquad (7)$$

326

327 R_0 under these assumptions is given by equation 8. It can be used to study the
328 trajectories of virulence evolution in diverse vector-parasite relationships. The parameter
329 values used in this study are provided in Table S1.

330

331 $$Ro = \frac{\theta_{\beta_{v\to h}}\frac{-1+\alpha_{21}}{-1+\alpha_{12}\alpha_{21}}}{\mu_v+\vartheta_v+\gamma_v}S_v * \frac{\theta_{\beta_{h\to v}}\theta_{\vartheta_h}\frac{-1+\alpha_{PE}}{-1+\alpha_{EP}\alpha_{PE}}}{\mu_h+\theta_{\vartheta_h}\frac{-1+\alpha_{PE}}{-1+\alpha_{EP}\alpha_{PE}}+\gamma_h}S_h \qquad (8)$$

332

333 **Mosquito rearing and parasite Infections**

334 *Anopheles gambiae s.l.* mosquitoes were used throughout the study. To prevent large
335 losses at early parasite stages (ookinetes) inflicted by the mosquito complement-like
336 system in the absence of Lp[21,46], all infection experiments were performed with immune-
337 deficient mosquitoes (*7b* line)[47]. G3 and *7b* mosquitoes, were maintained at 29°C 70%–
338 80% humidity 12/12 h day/night cycle. In *P. falciparum* infections, mosquitoes were fed
339 at 37°C for 15 min on a membrane feeder with NF54 gametocytes cultured with O+
340 human red blood cells (Haema, Berlin), and, thereafter, kept in a secured S3 laboratory
341 according to the national regulations (Landesamt für Gesundheit und Soziales, project
342 number 411/08). For *P. berghei* experiments, mosquitoes were fed on anesthetized CD1
343 mice infected with the GFP-expressing *P. berghei* GFP-con 259cl2 clone (ANKA
344 strain)[48]. Shortly after infections, unfed mosquitoes were removed, while fed mosquitoes
345 were maintained at 26°C for 11-14 days (*P. falciparum*) or at 20°C for 7-21 days (*P.*
346 *berghei*), and then used for the midgut and/or the salivary gland dissections.

347

348 **RNAi silencing**

349 Double stranded RNA (dsRNA) against *lipophorin* (*dsLp*) was produced as previously

350 described[21]. For RNAi silencing, 1-2 day-old females were anesthetized with CO_2 and
351 injected with 69 nl of 3 µg/µl *dsLacZ* (control) or *dsLp* using a Nanoject II Injector
352 (Drummond). Mosquitoes recovered for 3-4 days following injection before infections.
353 Efficiencies of RNAi silencing are summarized in Figure S8.

354

355 **Immunofluorescence analysis**

356 Mosquito midguts were dissected in PBS, fixed in 4% formaldehyde and washed in PBS.
357 Tissues were permeabilized with 0.1% Triton X-100 and incubated with a 1:1 mix of
358 mouse monoclonal anti-ApoI and anti-ApoII antibodies (1/300, clones 2H5 and 2C6)[21]
359 overnight at 4°C followed by incubation for 40 min at room temperature with the
360 secondary Cy3-labeled antibodies at 1/1,000 (Molecular Probes), or with 0.1 µg/ml of the
361 Nile Red stain (Sigma Aldrich). Nuclei were stained with DAPI (1.25 µg/ml, Molecular
362 Probes) for 40-60 min at room temperature. Images were acquired using an
363 AxioObserver Z1 fluorescence microscope equipped with an Apotome module (Zeiss).
364 Oocyst size was measured by hand-designing a circular ROI of randomly selected
365 oocysts (identified by GFP for *P. berghei* or by bright field and DAPI staining for *P.*
366 *falciparum*) using ZEN 2012 software (Zeiss). Images were then processed by FIJI
367 software (ImageJ 1.47m).

368

369 **Development of *P. berghei* liver-stages *in vitro***

370 The salivary glands of *P. berghei* infected mosquitoes were dissected, sporozoites were
371 collected into RPMI medium (Gibco) containing 3% bovine serum albumin (Sigma
372 Aldrich) and enumerated with a hemocytometer. The *P. berghei* liver stages were
373 cultured *in vitro* in HepG2 hepatoma cells and analyzed using standard techniques[49].
374 Briefly, 15,000 - 20,000 HepG2 cells per well (70% confluence) were plated on
375 transparent-bottom 96-wells plates (Nalgene International) and incubated for 24 h, then
376 seeded with 10,000 sporozoites and co-cultured at 37°C for 2 h. Free sporozoites were
377 removed by washing. As a negative control, sporozoites isolated from control
378 mosquitoes were pre-treated with the inhibitor of actin polymerization Cytochalasin D
379 (Sigma Aldrich) for 10 min. At 48 h post seeding, the cells were fixed with 4%
380 formaldehyde for 10 min, washed with PBS and blocked with 10% fetal calf serum in

381 PBS. Development of the liver-stage parasites was examined using monoclonal mouse
382 anti-GFP antibodies (1/1,000, AbCam) and revealed with the secondary AlexaFluor488
383 conjugated anti-mouse antibody (1/1,000, Molecular Probes). Nuclei were stained with
384 DAPI (1.25 µg/ml, Molecular Probes). Images were recorded directly on the 96-well plate
385 using an AxioObserver Z1 fluorescence microscope equipped with an Apotome module
386 (Zeiss) and analyzed for number and size of liver forms using the Axio-Vision ZEN 2012
387 software (Zeiss).

388

389 ***P. berghei* mouse infections *in vivo***

390 Mice were housed and handled in accordance with the German Animal Protection Law
391 (§8 Tierschutzgesetz) and both institutional (Max Planck Society) and national
392 regulations (Landesamt für Gesundheit und Soziales, registration number H 0027/12).
393 To determine infectivity to mice, the sporozoites collected from the mosquito salivary
394 glands were injected subcutaneously (5,000 sporozoites/mouse) into the tails of 8-10-
395 week-old C57BL/6 females. Bite-back experiments were performed by feeding the *P.*
396 *berghei*-infected mosquitoes (18 dpi) on anesthetized naïve C57BL/6 mice (mean 9
397 bites/mouse, range 2-15). Parasitemia was determined by daily Giemsa staining of thin
398 blood smears and FACS analysis of the red blood cells with the GFP-expressing blood
399 stage parasites. Infected mice were monitored every 6-12 h for the appearance of
400 severe neurological and behavioral symptoms typical of experimental cerebral malaria
401 (ECM) such as hunched body position, grooming alteration, ataxia, paralysis, or
402 convulsions[50] or by the rapid neurological and behavioral test (RMCBS)[51]. All mice with
403 ECM symptoms or the RMCBS score equal or below 5/20 were sacrificed immediately.

404

405 **Sporozoite imaging flow cytometry**

406 Salivary gland sporozoites were isolated into RPMI medium (Gibco) 3% bovine serum
407 albumin (Sigma Aldrich) and kept on ice until staining. Sporozoites were diluted in PBS
408 to concentrations corresponding to 3 mosquito equivalents and stained in the dark with
409 TMRE (5 nM) (Cell Signaling Technology) for 20 min at 20°C. Images were acquired
410 without washing using an ImageStreamX Mk II (Merck Millipore) with a 60x objective
411 over 1 h period. To avoid a possible bias due to the variable pre-acquisition waiting

412 times on ice, the order of sample acquisition was swapped between the experimental
413 replicates. GFP-expressing sporozoites were gated by size (Area_M01 or Area_M02)
414 and by GFP intensity (Intensity_MC_Ch02). The analysis was performed with IDEAS 6.2
415 (Merck Millipore) and FCS files were exported and analyzed by FlowJo v10. Given the
416 small size of the mitochondria, the feature finder tool from IDEAS software was used to
417 improve gating of optimally focused sporozoites. The following parameters were used to
418 discriminate in-focus single sporozoites from debris, and to identify in-focus sporozoites
419 to resolve their mitochondria: H Entropy Std_M01_Ch01_15 over H Variance
420 Std_M01_Ch01, Aspect Ratio_M02 over Symmetry 4-Object(M02_Ch2) Ch02, Gradient
421 RMS-M01-Ch01 over H Correlation Mean-M02-Ch02_3, and Gradient RMS-M02_Ch02.
422 Briefly, these parameters measure brightfield image texture, GFP image shape,
423 brightfield and GFP focus, respectively. For quantification of mitochondrial membrane
424 potential and GFP intensity, each sample was time-gated to exclude artefacts of
425 prolonged staining. The parameter corresponding to the lowest background signal in
426 unstained sporozoites was Bright Detail Intensity R7_M04_Ch04, Geo Mean which was
427 selected as *bona fide* TMRE intensity readout (see Figure S5D). For GFP intensity, the
428 Intensity_MC_Ch02, Geo. Mean was used. To validate the use of TMRE as a marker for
429 sporozoite membrane potential, we applied 50 μM of a mitochondrial uncoupling drug
430 CCCP (Cell Signaling Technology) and showed that drug treatment abolished TMRE
431 signal in sporozoites (see Figures S4D).

432

433 **Statistical analysis**

434 Statistical analysis was performed with GraphPad Prism 7 software and p values below
435 0.05 were considered significant (*: $p<0.05$; **: $p<0.001$; ***: $p<0.0001$) and indicated in
436 the figures. The specific tests used are indicated for each figure in the corresponding
437 legend.

438 **REFERENCES AND NOTES:**

439 1 WHO. *World Malaria Report 2016*. (Licence: CC BY-NC-SA 3.0 IGO., 2016).

440 2 Mideo, N., Day, T. & Read, A. F. Modelling malaria pathogenesis. *Cell Microbiol*
441 **10**, 1947-1955, doi:10.1111/j.1462-5822.2008.01208.x (2008).

442 3 Mideo, N. Parasite adaptations to within-host competition. *Trends Parasitol* **25**,
443 261-268, doi:10.1016/j.pt.2009.03.001 (2009).

444 4 Mideo, N. *et al.* Causes of variation in malaria infection dynamics: insights from
445 theory and data. *Am Nat* **178**, E174-188, doi:10.1086/662670 (2011).

446 5 Mackinnon, M. J. & Read, A. F. Genetic Relationships between Parasite
447 Virulence and Transmission in the Rodent Malaria Plasmodium Chabaudi.
448 *Evolution* **53**, 689-703, doi:10.1111/j.1558-5646.1999.tb05364.x (1999).

449 6 Sato, Y., Montagna, G. N. & Matuschewski, K. Plasmodium berghei sporozoites
450 acquire virulence and immunogenicity during mosquito hemocoel transit. *Infect*
451 *Immun* **82**, 1164-1172, doi:10.1128/IAI.00758-13 (2014).

452 7 Attardo, G. M., Hansen, I. A. & Raikhel, A. S. Nutritional regulation of
453 vitellogenesis in mosquitoes: implications for anautogeny. *Insect Biochem Mol*
454 *Biol* **35**, 661-675 (2005).

455 8 Maier, W. A., Becker-Feldman, H. & Seitz, H. M. Pathology of malaria-infected
456 mosquitoes. *Parasitol Today* **3**, 216-218 (1987).

457 9 Hogg, J. C. & Hurd, H. Malaria-induced reduction of fecundity during the first
458 gonotrophic cycle of Anopheles stephensi mosquitoes. *Med Vet Entomol* **9**, 176-
459 180 (1995).

460 10 Ferguson, H. M. & Read, A. F. Why is the effect of malaria parasites on mosquito
461 survival still unresolved? *Trends Parasitol* **18**, 256-261 (2002).

462 11 Ferguson, H. M., Mackinnon, M. J., Chan, B. H. & Read, A. F. Mosquito
463 mortality and the evolution of malaria virulence. *Evolution* **57**, 2792-2804 (2003).

464 12 Vezilier, J., Nicot, A., Gandon, S. & Rivero, A. Plasmodium infection decreases
465 fecundity and increases survival of mosquitoes. *Proc Biol Sci* **279**, 4033-4041,
466 doi:10.1098/rspb.2012.1394 (2012).

467 13 Vezilier, J., Nicot, A., Gandon, S. & Rivero, A. Plasmodium infection brings
468 forward mosquito oviposition. *Biol Lett* **11**, doi:10.1098/rsbl.2014.0840 (2015).

469 14 Bomze, I. Lotka–Volterra equation and replicator dynamics: a two-dimensional
470 classification. *Biological Cybernetics* **48**, 201–211 (1983).

471 15 Bomze, I. Lotka–Volterra equation and replicator dynamics: new issues in
472 classification. . *Biological Cybernetics* **72**, 447–453 (1995).

473 16 Alizon, S. & van Baalen, M. Transmission-virulence trade-offs in vector-borne
474 diseases. *Theor Popul Biol* **74**, 6-15, doi:10.1016/j.tpb.2008.04.003 (2008).

475 17 Mack, S. R. & Vanderberg, J. P. Plasmodium berghei: energy metabolism of
476 sporozoites. *Exp Parasitol* **46**, 317-322 (1978).

477 18 Ponnudurai, T. *et al.* Sporozoite load of mosquitoes infected with *Plasmodium*
478 *falciparum*. *Trans R Soc Trop Med Hyg* **83**, 67-70 (1989).

479 19 Pollitt, L. C. *et al.* Costs of crowding for the transmission of malaria parasites.
480 *Evol Appl* **6**, 617-629, doi:10.1111/eva.12048 (2013).

481 20 Atella, G. C., Bittencourt-Cunha, P. R., Nunes, R. D., Shahabuddin, M. & Silva-
482 Neto, M. A. The major insect lipoprotein is a lipid source to mosquito stages of
483 malaria parasite. *Acta Trop* **109**, 159-162, doi:S0001-706X(08)00272-
484 6[pii]10.1016/j.actatropica.2008.10.004 (2009).

485 21 Rono, M. K., Whitten, M. M., Oulad-Abdelghani, M., Levashina, E. A. & Marois,
486 E. The major yolk protein vitellogenin interferes with the anti-*Plasmodium*
487 response in the malaria mosquito *Anopheles gambiae*. *PLoS Biol* **8**, e1000434,
488 doi:10.1371/journal.pbio.1000434 (2010).

489 22 Ramakrishnan, C. *et al.* Salivary gland-specific *P. berghei* reporter lines enable
490 rapid evaluation of tissue-specific sporozoite loads in mosquitoes. *PLoS One* **7**,
491 e36376, doi:10.1371/journal.pone.0036376 (2012).

492 23 Perry, S. W., Norman, J. P., Barbieri, J., Brown, E. B. & Gelbard, H. A.
493 Mitochondrial membrane potential probes and the proton gradient: a practical
494 usage guide. *Biotechniques* **50**, 98-115, doi:10.2144/000113610 (2011).

495 24 Blandin, S. *et al.* Complement-like protein TEP1 is a determinant of vectorial
496 capacity in the malaria vector Anopheles gambiae. *Cell* **116**, 661-670,
497 doi:S0092867404001734 [pii] (2004).

498 25 Eickel, N. *et al.* Features of autophagic cell death in Plasmodium liver-stage
499 parasites. *Autophagy* **9**, 568-580, doi:10.4161/auto.23689 (2013).

500 26 Nguyen, T. B. *et al.* DGAT1-Dependent Lipid Droplet Biogenesis Protects
501 Mitochondrial Function during Starvation-Induced Autophagy. *Dev Cell* **42**, 9-21
502 e25, doi:10.1016/j.devcel.2017.06.003 (2017).

503 27 Boysen, K. E. & Matuschewski, K. Arrested oocyst maturation in Plasmodium
504 parasites lacking type II NADH:ubiquinone dehydrogenase. *J Biol Chem* **286**,
505 32661-32671, doi:10.1074/jbc.M111.269399 (2011).

506 28 Hino, A. *et al.* Critical roles of the mitochondrial complex II in oocyst formation
507 of rodent malaria parasite Plasmodium berghei. *J Biochem* **152**, 259-268,
508 doi:10.1093/jb/mvs058 (2012).

509 29 Oppenheim, R. D. *et al.* BCKDH: the missing link in apicomplexan mitochondrial
510 metabolism is required for full virulence of Toxoplasma gondii and Plasmodium
511 berghei. *PLoS Pathog* **10**, e1004263, doi:10.1371/journal.ppat.1004263 (2014).

512 30 Goodman, C. D. *et al.* Parasites resistant to the antimalarial atovaquone fail to
513 transmit by mosquitoes. *Science* **352**, 349-353, doi:10.1126/science.aad9279
514 (2016).

515 31 Davies, C. S., Pudney, M., Nicholas, J. C. & Sinden, R. E. The novel
516 hydroxynaphthoquinone 566C80 inhibits the development of liver stages of
517 Plasmodium berghei cultured in vitro. *Parasitology* **106 (Pt 1)**, 1-6 (1993).

518 32 Fowler, R. E., Sinden, R. E. & Pudney, M. Inhibitory activity of the anti-malarial
519 atovaquone (566C80) against ookinetes, oocysts, and sporozoites of Plasmodium
520 berghei. *J Parasitol* **81**, 452-458 (1995).

521 33 Azevedo, R. *et al.* A bioluminescence method for in vitro screening of
522 Plasmodium transmission-blocking compounds. *Antimicrob Agents Chemother*,
523 doi:10.1128/AAC.02699-16 (2017).

524 34 Goodman, C. D., Buchanan, H. D. & McFadden, G. I. Is the Mitochondrion a
525 Good Malaria Drug Target? *Trends Parasitol* **33**, 185-193,
526 doi:10.1016/j.pt.2016.10.002 (2017).

527 35 Gillies, M. T. The recognition of age-groups within populations of *Anopheles*
528 *gambiae* by the pre-gravid rate and the sporozoite rate. *Ann Trop Med Parasitol*
529 **48**, 58-74 (1954).

530 36 Takken, W. *et al.* Larval nutrition differentially affects adult fitness and
531 *Plasmodium* development in the malaria vectors *Anopheles gambiae* and
532 *Anopheles stephensi*. *Parasit Vectors* **6**, 345, doi:10.1186/1756-3305-6-345
533 (2013).

534 37 Moller-Jacobs, L. L., Murdock, C. C. & Thomas, M. B. Capacity of mosquitoes to
535 transmit malaria depends on larval environment. *Parasit Vectors* **7**, 593,
536 doi:10.1186/s13071-014-0593-4 (2014).

537 38 Shapiro, L. L., Murdock, C. C., Jacobs, G. R., Thomas, R. J. & Thomas, M. B.
538 Larval food quantity affects the capacity of adult mosquitoes to transmit human
539 malaria. *Proc Biol Sci* **283**, doi:10.1098/rspb.2016.0298 (2016).

540 39 Vantaux, A. *et al.* Larval nutritional stress affects vector life history traits and
541 human malaria transmission. *Sci Rep* **6**, 36778, doi:10.1038/srep36778 (2016).

542 40 Okech, B. A. *et al.* Influence of age and previous diet of *Anopheles gambiae* on
543 the infectivity of natural *Plasmodium falciparum* gametocytes from human
544 volunteers. *J Insect Sci* **4**, 33 (2004).

545 41 O'Keefe, K. J. & Antonovics, J. Playing by different rules: the evolution of
546 virulence in sterilizing pathogens. *Am Nat* **159**, 597-605, doi:10.1086/339990
547 (2002).

548 42 Mitchell, S. N. & Catteruccia, F. Anopheline Reproductive Biology: Impacts on
549 Vectorial Capacity and Potential Avenues for Malaria Control. *Cold Spring Harb*
550 *Perspect Med*, doi:10.1101/cshperspect.a025593 (2017).

551 43 Bourtzis, K. *et al.* Harnessing mosquito-Wolbachia symbiosis for vector and
552 disease control. *Acta Trop* **132 Suppl**, S150-163,
553 doi:10.1016/j.actatropica.2013.11.004 (2014).

554 44 Churcher, T. S. *et al.* Probability of Transmission of Malaria from Mosquito to
555 Human Is Regulated by Mosquito Parasite Density in Naive and Vaccinated
556 Hosts. *PLoS Pathog* **13**, e1006108, doi:10.1371/journal.ppat.1006108 (2017).

557 45 Schneider, P. *et al.* Submicroscopic Plasmodium falciparum gametocyte densities
558 frequently result in mosquito infection. *Am J Trop Med Hyg* **76**, 470-474 (2007).

559 46 Mendes, A. M. *et al.* Conserved mosquito/parasite interactions affect development
560 of *Plasmodium falciparum* in Africa. *PLoS Pathog* **4**, e1000069 (2008).

561 47 Pompon, J. & Levashina, E. A. A New Role of the Mosquito Complement-like
562 Cascade in Male Fertility in *Anopheles gambiae*. *PLoS Biol* **13**, e1002255,
563 doi:10.1371/journal.pbio.1002255 (2015).

564 48 Franke-Fayard, B. *et al.* A *Plasmodium berghei* reference line that constitutively
565 expresses GFP at a high level throughout the complete life cycle. *Mol Biochem*
566 *Parasitol* **137**, 23-33 (2004).

567 49 Silvie, O., Goetz, K. & Matuschewski, K. A sporozoite asparagine-rich protein
568 controls initiation of *Plasmodium* liver stage development. *PLoS Pathog* **4**,
569 e1000086, doi:10.1371/journal.ppat.1000086 (2008).

570 50 Lackner, P. *et al.* Behavioural and histopathological alterations in mice with
571 cerebral malaria. *Neuropathol Appl Neurobiol* **32**, 177-188, doi:10.1111/j.1365-
572 2990.2006.00706.x (2006).

573 51 Carroll, R. W. *et al.* A rapid murine coma and behavior scale for quantitative
574 assessment of murine cerebral malaria. *PLoS One* **5**,
575 doi:10.1371/journal.pone.0013124 (2010).
576

ACKNOWLEDGEMENTS

This work was supported by Max Planck Society, EC FP7 EVIMalaR (grant agreement n°242095) and MALVECBLOK (grant agreement nº223601). The authors thank H. Krüger, M. Andres and L. Spohr for mosquito rearing, mouse work assistance, and *Plasmodium* infections, and D. Tschierske and D. Eyermann for *P. falciparum* cultures. The authors express their gratitude to Prof. K. Matuschewski and his group for continuous fruitful discussions, to Dr. M.M. Mota and Dr. P. Carrillo-Bustamante for helpful comments.

AUTHOR CONTRIBUTIONS

GC and EAL conceived the study and designed the experiments. MG performed the modeling analysis. GC, ME, RL, CG, and VB performed experiments. AEH and RS contributed reagents and expertise. GC, ME, MG, RL, RS, CG, VB, and EAL analyzed the data. GC, MG and EAL wrote the manuscript.

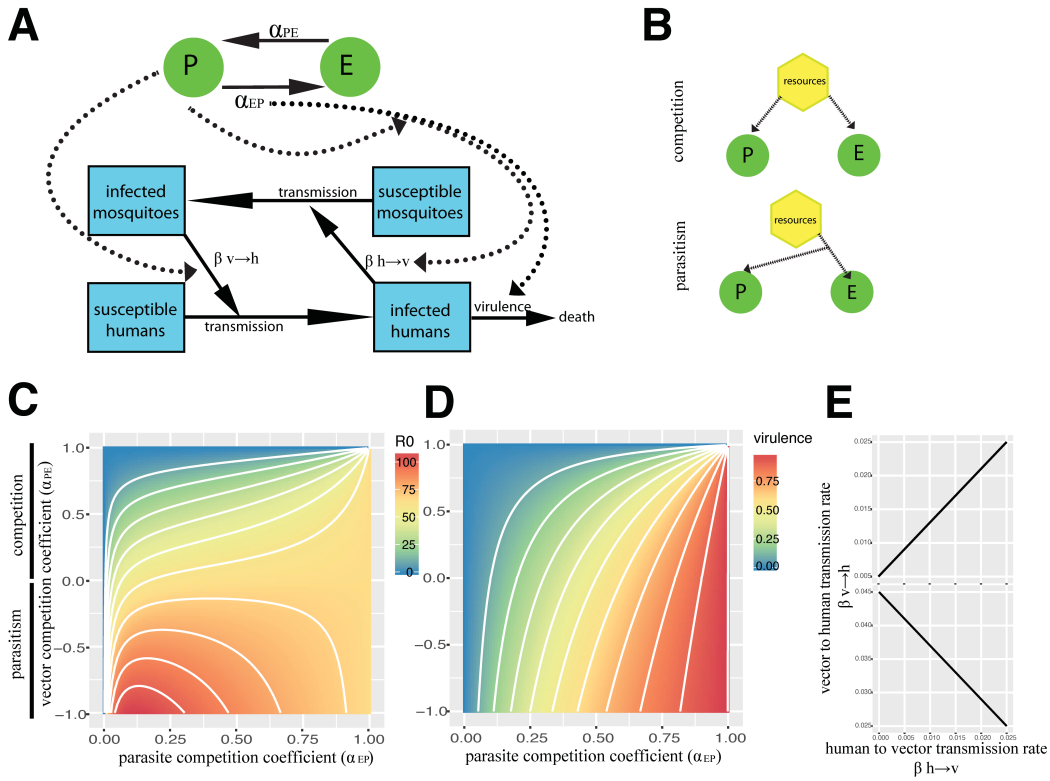

Figure 1. Evolution of vector-parasite antagonism and virulence.

(A) Model scheme of parasite-vector non-mutualistic symbiotic relationship (green), nested into epidemiological dynamics (blue): within-vector parasite density is positively linked to vector-to-human transmission, whereas human-to-vector transmission is a linear function of the parasite's virulence towards mosquito reproduction (competition coefficient) and human host longevity. **(B)** The biological relationship is competitive, if a common resource is scavenged, or parasitic if mosquito resource scavenging aids parasite development. **(C)** Contour plot of parasite fitness R_0 under varying within-vector interaction terms. The y-axis shows the relationship of mosquito egg production towards the parasite α_{PE} over the parasite's competition coefficient (i.e. virulence) α_{EP}. Positive values of α_{PE} showcase a competitive parasite-vector interaction, whereas negative values imply that vector reproduction benefits parasite density leading to a parasitic relationship. **(D)** Contour plot of parasite virulence towards the host under varying within-vector interaction terms. Under competitive scenario, parasite fitness increases with virulence, whereas under parasitic scenario, an evolutionarily stable virulence strategy

610 (ESV) emerges. **(E)** Vector-to-human transmission over human-to-vector transmission
611 under varying degrees of parasite virulence. When mosquito and parasites
612 independently scavenge and directly compete for resources (top, $\alpha_{PE} = 0.8$), the
613 transmission terms are positively linked. If parasites prey on mosquito resource
614 scavenging (bottom, $\alpha_{PE} = -0.8$), a trade-off between the transmission terms explains
615 the emergence of the ESV. P = parasites; E = mosquito eggs.

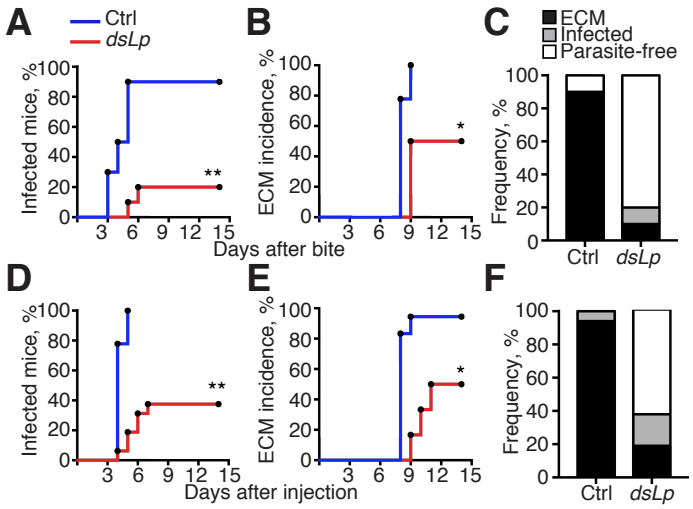

616
617
618 **Figure 2. Within-vector environment impacts within-host *Plasmodium* virulence.**
619
620 C57BL/6 mice infected by bites of *P.* berghei-infected mosquitoes (**A-C**) or by sporozoite
621 injection (**D-F**) were daily monitored for parasite occurrence in the blood and for
622 symptoms of experimental cerebral malaria (ECM). (**A**) Kaplan-Meier analysis of time to
623 infection (blood stage parasitaemia), (**B**) incidence (%) of experimental cerebral malaria
624 (ECM) and (**C**) cumulative health status of mice infected by bites of control (Ctrl, n=10)
625 or Lp-depleted (*dsLp*, n=10) mosquitoes. (**D**) Kaplan-Meier analysis of time to infection
626 (blood stage parasitaemia), (**E**) incidence (%) of experimental cerebral malaria (ECM)
627 and (**F**) cumulative health status of mice infected by subcutaneous injection of 5,000
628 sporozoites dissected from the salivary glands of control (Ctrl, n=18) or Lp-depleted
629 (*dsLp*, n=16) mosquitoes. Asterisks indicate statistically significant differences (*: $p<0.05$;
630 **: $p<0.001$; log-rank Mantel-Cox test and 2-way ANOVA).

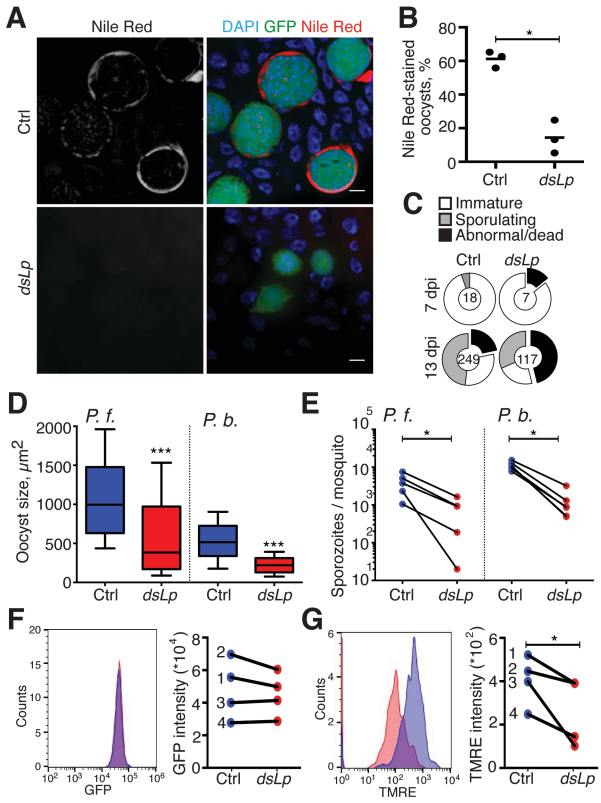

Figure 3. Mosquito lipids control within-vector oocyst proliferation, sporozoite metabolic activity and infectivity.

Control and Lp-deficient female mosquitoes were infected with *P. berghei* (*P.b.*) (**A-G**) or *P. falciparum* (*P.f.)* (**D**, **E**) parasites. (**A**) Neutral lipids detected by the Nile Red stain in the GFP-expressing *P. berghei* oocysts (green) 14 dpi in control (Ctrl) and Lp-depleted (*dsLp*) mosquitoes. Nuclei are visualized by DAPI (blue). Scale bars - 10 μm. (**B**) Percentage of Nile Red-positive *P. berghei* oocysts in control and Lp-depleted mosquitoes 13 dpi. At least 140 oocysts from 6 mosquitoes were analysed per condition. Each point represents mean of one experiment (n=3, *: $p<0.05$; paired t test). (**C**) Oocysts detected by transmission electron microscopy (see also Figure S3) were scored according to the developmental stage: non-sporulating oocysts with normal morphology (immature, white); oocysts with normal plasma membrane retraction, budding sporoblasts, or formed sporozoites (sporulating, gray); oocysts with aberrant electron-light intracellular vacuolization (abnormal/dead, black). Proportions of the categories are shown as pie charts and the total number of analyzed oocysts per condition is indicated in the middle of each chart. (**D**) Differences in oocyst sizes of *P.f.* (11 dpi, n=3) and *P.b.*

650 (14 dpi, n=6) in control and Lp-depleted mosquitoes. At least 225 oocysts were
651 measured per condition. The box plots represent medians (horizontal bars) with 10th
652 and 90th percentiles. (***: $p<0.0001$, Mann-Whitney test). (**E**) Development of *P.f.* (14
653 dpi, n=5) and *P.b.* (18 dpi, n=4) salivary gland sporozoites in control and Lp-depleted
654 mosquitoes. Each point represents the mean number of sporozoites per mosquito for
655 each experimental replicate. Asterisks indicate statistically significant differences (*:
656 $p<0.05$; 2-way ANOVA). Sporozoite (**F**) GFP expression and (**G**) mitochondrial
657 membrane potential as measured by TMRE were analysed using imaging flow
658 cytometry. Histograms from one representative experiment (left panels) and geometrical
659 mean values from four independent experiments (right panels) in control (blue, n=1,405)
660 and lipid-deprived (red, n=593) sporozoites are shown. Asterisks indicate statistically
661 significant differences (*: $p<0.05$; paired t test).

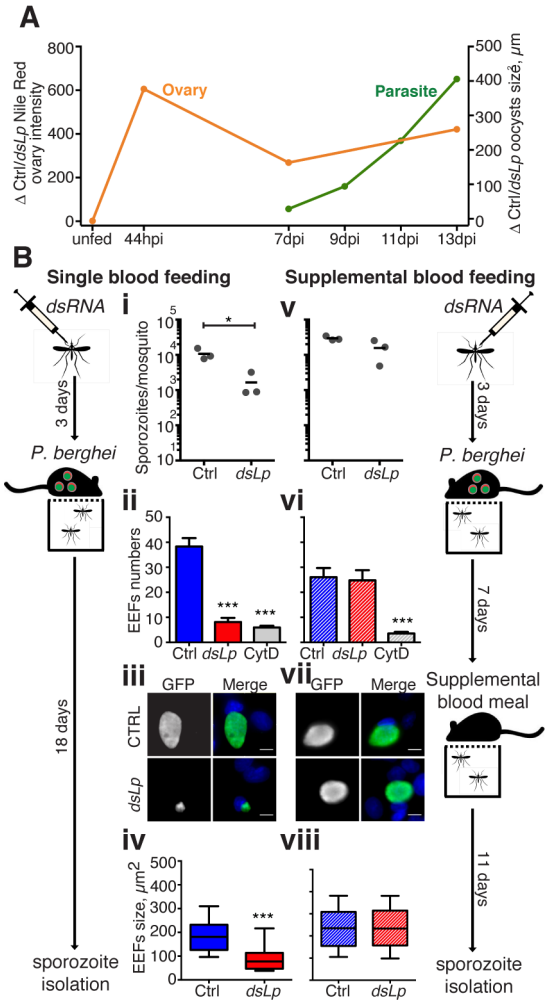

Figure 4. *Plasmodium* time-shift in sporulation circumvents competition for mosquito resources.

(**A**) Kinetics of lipid acquisition by mosquito ovaries and *P. berghei* oocyst development. The ratios of Nile Red mean intensities in the ovaries (orange line) and oocysts growth (green line) between control and Lp-depleted mosquitoes are shown. Five or more mosquitoes were dissected per time point per condition (n≥2). (**B**) Lp-depleted mosquitoes (*dsLp*) and controls (Ctrl) were infected with *P. berghei* and offered (**v-viii**) or not (**i-iv**) a supplemental blood meal 7 days post infection. Salivary gland sporozoites were isolated and counted from control and Lp-deficient mosquitoes (**i** and **v**). Human hepatoma HepG2 cells were infected with 10,000 sporozoites and the number of extra-erythrocytic forms (EEFs) per field was gauged by microscopy 2 dpi (**ii** and **vi**). As a

676 negative control, sporozoites from control mosquitoes were treated with cytochalasin D
677 (Cyt D). Mean numbers and SEM are shown. Representative fluorescent micrographs of
678 GFP-expressing EEFs (green) developing in HepG2 cells (**iii** and **vii**). Cell nuclei are
679 stained with DAPI (blue). Scale bar - 10 μm. EEF sizes produced by sporozoites from
680 control and Lp-deficient mosquitoes (**iv** and **viii**). The box plots represent 10th and 90th
681 percentiles while the horizontal lines show medians. Asterisks indicate statistically
682 significant differences (n=3, *: $p<0.05$; ***: $p<0.0001$; Kruskal-Wallis and Mann-Whitney
683 test).